

Lattice effects on ferromagnetism in perovskite ruthenates

J.-G. Cheng, J.-S. Zhou*, and J.B. Goodenough†

The Materials Science and Engineering Program/ Mechanical Engineering, University of Texas at Austin, Austin, Texas 78712, USA

Ferromagnetism and its evolution in the orthorhombic perovskite system $Sr_{1-x}Ca_xRuO_3$ have been widely believed to correlate with the structural distortion. The recent development of high-pressure synthesis of the Ba substituted $Sr_{1-y}Ba_yRuO_3$ makes it possible to study ferromagnetism over a broader phase diagram, which includes new orthorhombic *Imma* and the cubic phases. However, the chemical substitutions introduce the A-site disorder effect on T_c , which complicates determination of the relationship between ferromagnetism and the structural distortion. By clarifying the site disorder effect on T_c in several new series of ruthenates in which the average bond length $\langle A-O \rangle$ keeps the same, but the bond-length variance varies, we are able to demonstrate a parabolic curve of T_c versus mean bond length $\langle A-O \rangle$. A much higher $T_c \approx 177$ K than that found in orthorhombic $SrRuO_3$ can be obtained from the curve at a bond length $\langle A-O \rangle$ which makes the geometric factor $t = \langle A-O \rangle / (\sqrt{2}\langle Ru-O \rangle) \approx 1$. This new result reveals not only that the ferromagnetism in the ruthenates is extremely sensitive to the lattice strain, but also that it has an important implication for exploring the structure-property relationship in a broad range of oxides with perovskite or perovskite-related structure.

The A-site cation in conductive transition-metal oxides AMO_3 with a perovskite or a perovskite-related structure does not contribute directly to the density of electronic states near the Fermi energy. However, both the superconductive transition temperature T_c in the cuprates (1, 2) and the ferromagnetic transition temperature T_c in the magnetoresistive manganites (3) are highly sensitive to the A-cation disorder as well as the mean A-cation radius $\langle r_A \rangle$ in these mixed-valent systems. The lattice effects are

greatly enhanced in manganites where the ferromagnetic transition is accompanied by a first-order metal-insulator transition. Ferromagnetism in the orthorhombic perovskite SrRuO₃ and its unusual disappearance in isostructural CaRuO₃ (4-8) have not been well-understood. Early band structure calculations indicated that the orthorhombic distortion is critical for the electronic structure that supports ferromagnetism in both SrRuO₃ and CaRuO₃.(9) Mazin and Singh (10) have argued from their first-principles calculation that the orthorhombic distortion in CaRuO₃ is responsible for a much reduced $N(E_F)$ and the suppression of ferromagnetism. On the other hand, they have found an unusually high $N(E_F)$ in the cubic phase that can lead to instabilities. The small orthorhombic distortion found in SrRuO₃ was considered nearly ideal to stabilize ferromagnetism. In a recent calculation, Middey *et al* (11) have further argued that an optimum T_c in the perovskite ruthenates would occur in the orthorhombic phase where the GdFeO₃-type distortion is small. An enlarged orthorhombic distortion and smaller cell volume was found to destroy ferromagnetism in CaRuO₃. These models have been used to explain qualitatively the experimental phase diagram of T_c versus $\langle r_A \rangle$ for Sr_{1-x}Ca_xRuO₃ available in the literature. Extending the phase diagram to the Ba-substituted side brings a new test to our existing understanding. Recent progress in the high-pressure synthesis of Sr_{1-y}Ba_yRuO₃ has demonstrated the entire evolution of the ferromagnetic phase all the way to BaRuO₃.(12) Unlike the rare-earth substitution in RMO₃ perovskite systems, the change from Ca to Sr and to Ba introduces a relatively large change of $\langle r_A \rangle$ in addition to a slightly different chemical property between them. Combinations between these three elements make possible a continuous change of $\langle r_A \rangle$; but it also introduces the size variance effect on T_c . It is therefore not clear whether T_c truly peaks out at the $\langle r_A \rangle$ for SrRuO₃ as shown by an experimental phase diagram of A_{1-x}A'_xRuO₃ (A,A' =Ca, Sr, Ba) (12) and as expected by first-principles calculations. In order to obtain how T_c is correlated to the crystal structure, which is essential for understanding ferromagnetism in ruthenates, we have made a systematic study of the size variance effect on T_c . This study leads to a new phase diagram of T_c versus the average $\langle A-O \rangle$ bond length without influence from the bond-length variance. These new results indicate that the current understanding about ferromagnetism in ruthenates is incomplete.

We used the following procedure to introduce the A-cation size variance. The tabulated ionic radii depend sensitively on the coordination number (13) and they have been found to be not compatible with structures determined by the state-of-the-art neutron diffractions in recent years. Moreover, the O^{2-} ion should not be treated as a hard sphere. We have chosen the bond lengths obtained experimentally on perovskite ruthenates as listed in Table I.(12, 14, 15) One may be concerned that the bond length $\langle Ba-O \rangle = 2.832 \text{ \AA}$ from a cubic $BaRuO_3$ is under compression whereas the $\langle Ru-O \rangle = 2.003 \text{ \AA}$ is under tension (12); therefore, some adjustment may be needed in order to have the equilibrium mean bond length for calculating the $\langle A-O \rangle$ for other compositions with the Ba substitution. First of all, we have no basis for the adjustment. Second, it may also not be necessary since the substituted Ba would create the same local lattice strain as in a cubic $BaRuO_3$. As a matter of fact, all compositions having a Ba component need to be synthesized under pressure regardless of their $\langle A-O \rangle$ relative to $\langle Sr-O \rangle$, which may justify that we have used $\langle Ba-O \rangle = 2.832 \text{ \AA}$ from a high-pressure product $BaRuO_3$ for calculating the $\langle A-O \rangle$ for other compositions. We have obtained essentially the same conclusion by using the $\langle A-O \rangle$ bond length either from experiment or the tabulated value. In order to have all samples made under the same conditions, we have also made $SrRuO_3$ by high-pressure synthesis. T_c of the high-pressure-synthesized (HP) $SrRuO_3$ increases by 4 K and the moment at 5 K reaches $1.6 \mu_B$ under 5 T, which is equivalent to its value at 44 T for a sample prepared at ambient pressure.(16) Based on the bond lengths in Table I, a combination of $0.51\langle Ca-O \rangle$ and $0.49 \langle Ba-O \rangle$ is equal to $\langle Sr-O \rangle$. Therefore, the substitution of $Ba_{.49}Ca_{.51}$ for Sr in $Sr_{1-x}(Ba_{.49}Ca_{.51})_xRuO_3$ does not change the mean A-O bond length $\langle A-O \rangle = \langle Sr-O \rangle$, but it changes the bond-length variance defined as $\sigma^2 = \sum a_i L_i^2 - (\sum a_i L_i)^2$. The Sr concentration in $Sr_{1-x}Ca_xRuO_3$ and $Sr_{1-y}Ba_yRuO_3$ has been progressively replaced by $Ba_{.49}Ca_{.51}$; therefore the bond-length variance can be varied in a series of ruthenates for a given constant $\langle A-O \rangle$. The pressure required for synthesizing a single phase sample increases with increasing overall Ba concentration. At $P = 15 \text{ GPa}$, the highest pressure in this study, the maximum concentration of $(Ba_{.49}Ca_{.51})$ substitution for Sr in $Sr_{1-x}Ca_xRuO_3$ is 0.35 for $SrRuO_3$; its substitution for Sr in $Sr_{1-y}Ba_yRuO_3$ progressively decreases.

Fig.1 shows the temperature dependence of magnetic susceptibility χ for some typical ruthenates. While the paramagnetic $\chi^{-1}(T)$ of SrRuO₃ and the Ba substituted Sr_{1-y}Ba_yRuO₃ fulfills the typical Curie-Weiss law, an anomaly in $\chi^{-1}(T)$, pointed by an arrow, can be found in the paramagnetic phase of Sr_{1-x}Ca_xRuO₃ at $T > T_c$. A similar anomaly has also been observed by He *et al* (6) for members of the Sr_{1-x}Ca_xRuO₃ system. Although T_c is reduced as the bond-length variance is introduced, for example, in the series Sr_{1-x}(Ba_{.49}Ca_{.51})_xRuO₃ with $\langle A-O \rangle = \langle Sr-O \rangle$, the paramagnetic $\chi(T)$ can be well-described by the Curie-Weiss law. T_c in these samples is defined to be where $d\chi(T)/dT$ shows a peak.

We start the discussion of the bond-length variance effect from the series of Sr_{1-x}(Ba_{.49}Ca_{.51})_xRuO₃ with $\langle A-O \rangle = \langle Sr-O \rangle = 2.78 \text{ \AA}$; the bond-length variance σ^2 increases with x . As shown in Fig.2, T_c decreases linearly with increasing σ^2 as described by the formula $T_c = T_c^0 - p\sigma^2$, where T_c^0 is the Curie temperature of the sample without the bond-length variance. The local disorder due to the bond-length variance introduces perturbations that are normally harmful for a long-range ordered state. Interestingly, the same bond-length variance effect on transition temperature T_c has been found in both the high- T_c cuprates and the ferromagnetic manganites R_{1-x}A_xMnO₃ where R is a rare-earth, A is an alkaline earth (after the size variance is converted into the bond-length variance) (1, 3) We have also synthesized a series of ruthenates with $\langle A-O \rangle \neq \langle Sr-O \rangle$ and having different σ^2 . The same linear behavior of T_c versus σ^2 has also been found in these series of samples. The difference is that the T_c^0 from the linear fitting can be compared directly with experiment only for the series with $\langle A-O \rangle = \langle Sr-O \rangle = 2.78 \text{ \AA}$. For a series with $\langle A-O \rangle \neq \langle Sr-O \rangle$, T_c^0 can be obtained by extrapolating lines to $\sigma^2 = 0$. It should be noticed that lines fitting T_c versus σ^2 for the whole series are nearly parallel to each other. Therefore, the averaged slope p from lines with multiple points can be used to predict T_c^0 for the series where only one or two points of (T_c, σ^2) are available. These results allow us to map out T_c^0 versus $\langle A-O \rangle$ for the entire family of perovskites ARuO₃ in Fig.3(a). It is clear that $T_c^0 = T_c$ for SrRuO₃ is no longer located at a maximum in the new phase diagram. The overall evolution of T_c^0 versus $\langle A-O \rangle$ can be fit nearly perfectly by a

quadratic formula $T_c^0 = T_c^m - q(L^m - \langle A-O \rangle)^2$. The curve fitting gives a $T_c^0 = 0$ at $\langle A-O \rangle \approx 2.74 \text{ \AA}$ where the T_c onset has been found experimentally. On the other side of the dome, it is difficult to verify the point of $T_c^0 = 0$ at $\langle A-O \rangle \approx 2.842 \text{ \AA}$ since an element like Ra with $\langle Ra-O \rangle > \langle Ba-O \rangle$ is required. The maximum $T_c^0 \approx 177 \text{ K}$, much higher than $T_c \approx 164 \text{ K}$ for SrRuO_3 , occurs at $\langle A-O \rangle \approx 2.791 \text{ \AA}$. Fitting to a quadratic formula indicates that the lattice strain plays a role in the ferromagnetism of the perovskite ruthenates. In order to understand why T_c peaks out at an $\langle A-O \rangle > \langle Sr-O \rangle$ and why a lattice strain formula fits well the curve of T_c versus $\langle A-O \rangle$, we turn to the results of our structural study.

In contrast to the Ca substituted samples $\text{Sr}_{1-x}\text{Ca}_x\text{RuO}_3$, which can be synthesized under ambient pressure, the crystal structures of the high-pressure products $\text{Sr}_{1-y}\text{Ba}_y\text{RuO}_3$ have not been refined systematically until this work. Our new results, shown in Fig.3(b), complete the structural phase diagram of the perovskites ARuO_3 ; all detailed structural parameters from refinements and typical results can be found in the Supplement Materials. Due to the well-known octahedral-site distortion,(17) the lattice parameter b crosses a in the orthorhombic $Pbnm$ phase of $\text{Sr}_{1-x}\text{Ca}_x\text{RuO}_3$. The lattice parameter $b > a$ holds for the $Pbnm$ phase with rigid octahedra as predicted by using the software SPuDS; the prediction is also shown as the dashed lines in the Fig.3(b). The lattice parameter crossing also serves as a precursor for the phase transition to the $Imma$ phase, which is commonly found in other $A^{2+}B^{4+}O_3$ perovskite families between the orthorhombic $Pbnm$ phase and the cubic $Pm-3m$ phase.(18, 19) It is clear from comparison of Fig.3 (a) and (b) that the orthorhombic $Imma$ phase offers the highest T_c . The continuous change of lattice parameters versus $\langle A-O \rangle$ on crossing from the $Pbnm$ to $Imma$ and finally to the $Pm-3m$ phase offers no useful information to explain why ferromagnetism prefers the $Imma$ phase. By refining XRD patterns, we have further resolved the dependences of the bond length Ru-O and the bond angle Ru-O-Ru versus $\langle A-O \rangle$ in Fig.3(c). The bond-length mismatch in the $Pbnm$ phase due to the geometric tolerance factor $t \equiv (A-O)/\sqrt{2}(B-O) < 1$ places the Ru-O bond under compression, which directly leads to the cooperative octahedral-site rotation and therefore to reduction of the Ru-O-Ru bond angle from 180° . On the other hand, the Ru-O bond is stretched in the cubic phase as $\langle A-O \rangle$ increases with

the Ba substitution in $\text{Sr}_{1-y}\text{Ba}_y\text{RuO}_3$. The overall variation of the Ru-O bond length as a function of $\langle\text{A-O}\rangle$ is within $\pm 0.01 \text{ \AA}$, which actually reaches the resolution limit for the refinement of XRD patterns in this study. However, the Ru-O-Ru bond angle just reaches 180° at the *Imma*/*Pm-3m* phase boundary where the Ru-O bond is under neither a compressive nor a stretching stress. By taking the $\langle\text{A-O}\rangle_m = 2.795 \text{ \AA}$ from the parabolic curve fitting and the experimental $\langle\text{Ru-O}\rangle_m \approx 1.980 \text{ \AA}$ in Fig.3, we found that the maximum T_c^0 occurs at $t = 0.998$. It is interesting to notice that the Ru-O bond length undergoes a minimum at $t \approx 1$. A similar observation has been made in the (Ca,Sr,Ba)SnO₃ system. (18) Instead of a cubic structure, the orthorhombic *Imma* structure corresponding to $t \approx 1$ must be related to the bond-length variance for the composition. Ferromagnetism in the ruthenates appears to prefer the phase with a nearly equilibrium Ru-O bond length. The bond-length analysis is highly consistent with the fit of T_c versus $\langle\text{A-O}\rangle$ to a quadratic formula, indicating a lattice strain effect, which is missing in the first-principles calculations. The calculation based on an itinerant-electron model predicted a Fermi surface instability as the cubic phase is approached.(10, 11) Therefore, a maximum T_c should occur in a slightly distorted *Pbnm* phase. This argument is not supported by our experimental results.

As shown in Fig.1, the paramagnetic susceptibility and its behavior in the vicinity of T_c in the Ca-substituted $\text{Sr}_{1-x}\text{Ca}_x\text{RuO}_3$ is remarkably different from that of the Ba substituted $\text{Sr}_{1-y}\text{Ba}_y\text{RuO}_3$, which exhibits a typical Curie-Weiss behavior at all $T > T_c$. The reduction of $\chi^{-1}(T)$ of $\text{Sr}_{1-x}\text{Ca}_x\text{RuO}_3$ as T_c is approached in the paramagnetic phase is stunningly similar to that of a Griffiths phase.(20, 21) This observation has led to a scenario that the T_c reduction as x increases in $\text{Sr}_{1-x}\text{Ca}_x\text{RuO}_3$ is due to a dilution effect by non-magnetic ions. Given that SrRuO_3 showing the Curie-Weiss $\chi^{-1}(T)$ falls on the same side of the dome as the Ca substituted samples from our new results in Fig.3(a), the Griffiths dilution story is not sufficient to explain the T_c reduction at $\langle\text{A-O}\rangle < 2.795 \text{ \AA}$. The covalent competition between the A-O bond and the B-O bond in the perovskite structure could be another factor to influence Curie temperature. In the perovskites ARuO_3 , the A-O σ bond competes for the O-2p electron that π bonds with the Ru. On the Ba-substituted side, the more basic Ba-O bond competes less strongly for the common O-2p electron,

which strengthens the Ru-O π bonding and can broaden the π^* band despite a stretching of the Ru-O bond length. T_c decreases with increasing bandwidth in an itinerant-electron ferromagnet. While these effects may influence T_c in higher orders, the model fails to account for a maximum T_c occurring in the *Imma* phase and for an overall profile of T_c versus $\langle A-O \rangle$.

While the lattice strain story explains the overall observations of T_c versus $\langle A-O \rangle$ and the Ru-O bond stress due to the bonding mismatch in the perovskite structure, it is still difficult to account for the pressure dependence of T_c in cubic BaRuO₃.(22) The Ru-O bond in BaRuO₃ is highly stretched and T_c is reduced to about 60 K. T_c would increase under high pressure based on the lattice strain story since pressure reduces the Ru-O bond length without bending the Ru-O-Ru bond angle from 180°. However, we have found that T_c in BaRuO₃ decreases dramatically under pressure and BaRuO₃ becomes a paramagnetic metal down to 2 K under $P = 8$ GPa. This discrepancy reflects that a higher compressibility of the $\langle Ba-O \rangle$ bond than the $\langle Ru-O \rangle$ bond, which increases the Ru-O covalent bonding to broaden the RuO₂ π^* band. A similar discrepancy has been observed in high- T_c cuprates. In the plot of T_c versus $\langle r_A \rangle$ for the cuprates with a single CuO₂ layer, HgBa₂CuO₄ is located at the maximum on the parabolic curve.(2) A $dT_c/dP < 0$ can be predicted from this plot. However, experiment has shown that T_c increases under pressure.(23)

From symmetry considerations in a band model,(10) the highest density of states $N(E_F)$ can be obtained in the cubic phase due to the high state degeneracy. On the other hand, the data for the Ru-O bond length and the Ru-O-Ru bond angle ϕ in Fig.3(c) show an abrupt increase in $\langle Ru-O \rangle$ on entering the *Pbnm* phase where a cooperative rotation of the RuO₆ octahedra reduces the Ru-O-Ru bond angle from 180°. The increase in $\langle Ru-O \rangle$ would appear to relax the elastic strain on the bond, but the equilibrium $\langle Ru-O \rangle$ bond length would be increased by the introduction of localized 4d electrons, which have a larger volume. The ferromagnetism of the Ru-4d electrons signals that the π^* bands are narrow and approach the crossover to the localized-electron state where a large spin-orbit

coupling creates a localized-electron state with a reduced total magnetic moment below the Griffiths anomaly. The jump in the $\langle \text{Ru-O} \rangle$ bond length in the $Pbnm$ phase together with the appearance of the Griffiths phase anomaly in the susceptibility is consistent with the coexistence below the Griffiths temperature of localized-electron clusters that grow in volume with increasing x in the $\text{Sr}_{1-x}\text{Ca}_x\text{RuO}_3$ system as the crossover to localized-electron behavior is approached from the itinerant electron side. The transition from a narrow itinerant-electron band to a localized-electron phase is commonly first-order and characterized by a coexistence two phases if not by stabilization of a charge-density wave. The existence of ferromagnetic order in the itinerant-electron phase can be expected to suppress formation of a spin-paired charge-density wave. The dilution in spin-spin interactions is caused by localized-electron clusters with an enhanced spin-orbit coupling that alters the spin-spin interactions responsible for the ferromagnetic itinerant-electron phase. This observation and the lattice strain effect on T_c must be taken into account in modeling the mysterious ferromagnetism in perovskite ruthenates.

In conclusion, the availability of $\text{Sr}_{1-y}\text{Ba}_y\text{RuO}_3$ synthesized under high pressure extends the ferromagnetic phase into the orthorhombic $Imma$ and cubic $Pm-3m$ phases. We have shown that T_c decreases linearly with the bond-length variance σ^2 in both $\text{Sr}_{1-y}\text{Ba}_y\text{RuO}_3$ and $\text{Sr}_{1-x}\text{Ca}_x\text{RuO}_3$. A ferromagnetic transition temperature T_c^0 without the influence from the bond-length variance can be obtained for SrRuO_3 and BaRuO_3 and for $\langle r_A \rangle$ other than $A = \text{Sr}$ and Ba by extrapolating T_c versus σ^2 to $\sigma^2=0$. The curve T_c^0 versus mean bond length $\langle A-O \rangle$ can be fit with a quadratic formula, which indicates that a lattice strain effect plays a dominant role in controlling the ferromagnetic transition of perovskite ruthenates. A maximum T_c can be obtained in a perovskite ruthenate with the geometric tolerance factor $t = 1$ where the unstrained Ru-O bond length with 180° Ru-O-Ru bond angle is found.

Materials and Methods

The high-pressure syntheses were carried out in a Walker-type multianvil module (Rockland Research). All samples were examined with powder X-ray diffraction (XRD) at room temperature with a Philips X'pert diffractometer (Cu $K\alpha$ radiation). Lattice

parameters were obtained by using the least-square analysis with the software *Jade* and the Rietveld refinement method with the software *Fullprof*. Magnetic properties were measured with a superconducting quantum interference device (SQUID) magnetometer (Quantum Design).

Acknowledgements

The work was supported by NSF (DMR 1122603) and the Robert A. Welch foundation (Grant F-1066).

* jszhou@mail.utexas.edu

† jgoenough@mail.utexas.edu

Author contributions: all authors designed the research and wrote the paper; JGC and JSZ performed the materials synthesis, characterization, and analyzed the data.

Table I Experimental <A-O> bond lengths obtained on perovskite ruthenates ARuO₃

ARuO ₃	<A-O> (Å)	<Ru-O> (Å)	References
A = Ca	2.728	1.992	14
A = Sr	2.780	1.984	15
A = Ba	2.832	2.003	12

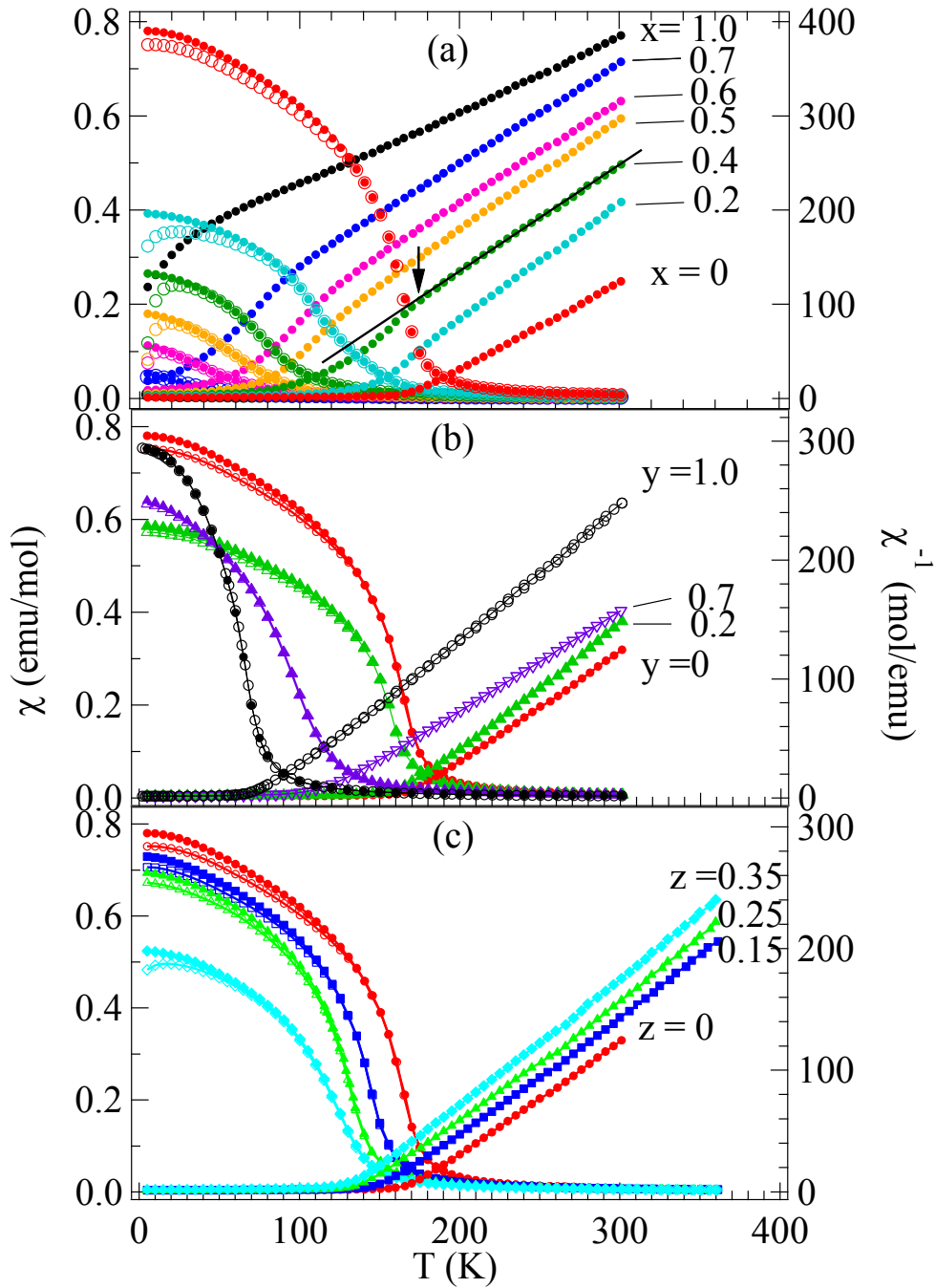


Fig. 1 Temperature dependences of magnetic susceptibility χ and χ^{-1} for (a) $\text{Sr}_{1-x}\text{Ca}_x\text{RuO}_3$; (b) $\text{Sr}_{1-y}\text{Ba}_y\text{RuO}_3$; (c) $\text{Sr}_{1-z}(\text{Ba}_{0.49}\text{Ca}_{0.51})_z\text{RuO}_3$. All measurements were performed with $H = 1$ T; open symbols are for zero-field-cool and solid symbols are for field cool. The arrow in (a) indicates the temperature where the $\chi^{-1}(T)$ deviates from a Curie-Weiss fitting in the paramagnetic phase.

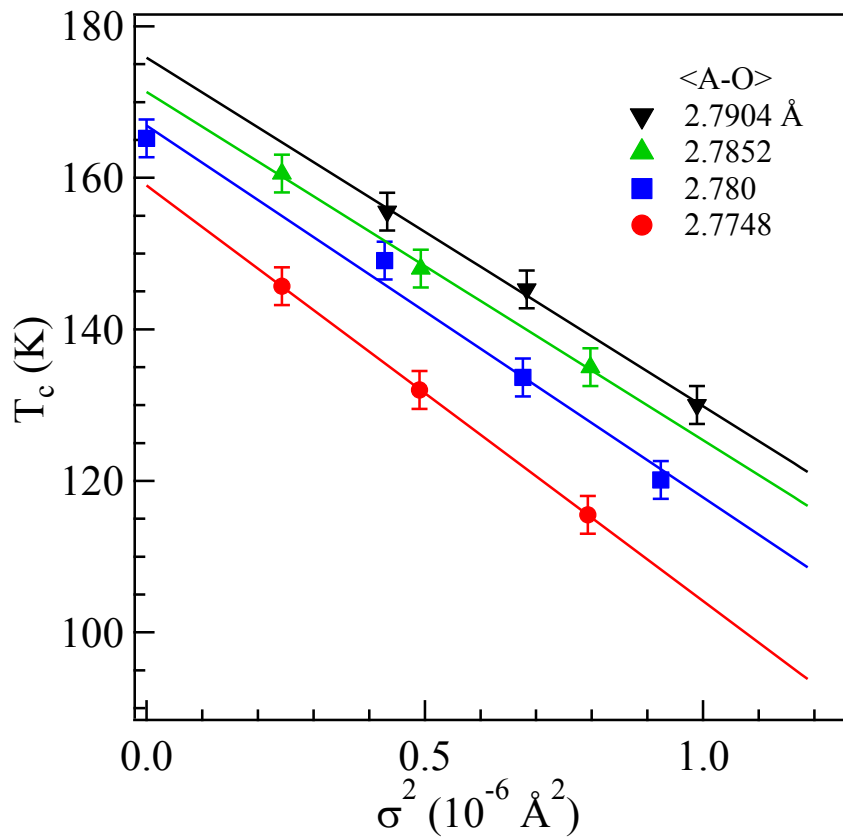


Fig.2 Ferromagnetic transition temperature T_c versus the bond-length variance σ^2 for several series of perovskite ruthenates with different mean A-O bond length. Lines inside figure are results of linear fitting to the data.

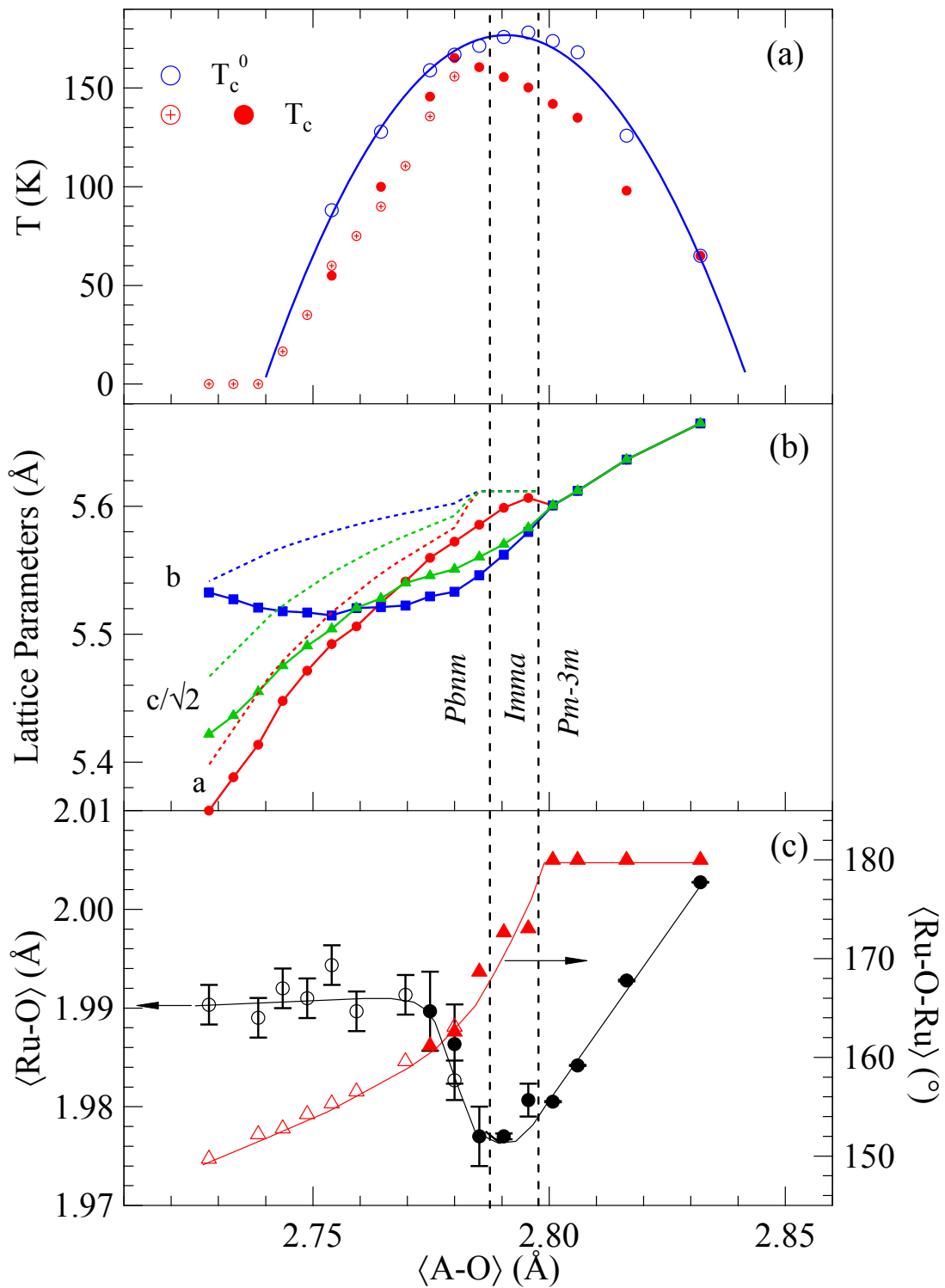


Fig.3 (a) The phase diagram of T_c and T_c^0 (see the text for the definition) versus the mean A-O bond length $\langle A-O \rangle$. The solid symbol is for the samples synthesized under

high pressure; the circle and plus symbol is for the samples synthesized under ambient pressure. (b) lattice parameters versus $\langle A-O \rangle$ on crossing three crystal structures (we have converted lattice parameters from all other phases into the *Pbnm* structure for clarification). The dashed lines are lattice parameters calculated with SPuDS. (c) the Ru-O bond length and the Ru-O-Ru bond angle versus $\langle A-O \rangle$ in which data in open symbols are from ref.8 and those in solid symbols are from this work.

1. Atfield JP, Kharlanov AL, & McAllister JA (1998) Cation effects in doped La_2CuO_4 superconductors. *Nature* 394:157-159.
2. Hobou H, *et al.* (2009) Enhancement of the superconducting critical temperature in $\text{Bi}_2\text{Sr}_2\text{CaCu}_2\text{O}_{8+\delta}$ by controlling disorder outside CuO_2 planes. *Phys Rev B* 79(6):064507.
3. Rodriguez-Martinez LM & Atfield JP (1996) Cation disorder and size effects in magnetoresistive manganese oxide perovskites. *Phys Rev B* 54(22):R15622-R15625.
4. Longo JM, Raccach PM, & Goodenough JB (1968) Magnetic properties of SrRuO_3 and CaRuO_3 . *J Appl Phys* 39:1327-1328.
5. Cao G, McCall S, Shepard M, Crow JE, & Guertin RP (1997) Thermal, magnetic, and transport properties of single-crystal $\text{Sr}_{1-x}\text{Ca}_x\text{RuO}_3$ ($0 \leq x \leq 1.0$). *Phys Rev B* 56:321-329.
6. He T, Huang Q, & Cava RJ (2000) Comparison of the magnetic properties of isoelectronic $\text{Sr}_x(\text{Na}_{0.5}\text{La}_{0.5})_{1-x}\text{RuO}_3$ and $\text{Sr}_x\text{Ca}_{1-x}\text{RuO}_3$ perovskites. *Phys Rev B* 63(2):024402.
7. Yoshimura K, *et al.* (1999) ^{17}O NMR observation of universal behavior of ferromagnetic spin fluctuations in the itinerant magnetic system $\text{Sr}_{1-x}\text{Ca}_x\text{RuO}_3$. *Phys Rev Lett* 83(21):4397-4400.
8. Kobayashi H, Nagata M, Kanno R, & Kawamoto Y (1994) Structural characterization of the orthorhombic perovskites: ARuO_3 (A = Ca, Sr, La, Pr). *Mat Res Bull* 29(12):1271-1280.
9. Santi G & Jarlborg T (1997) Calculation of the electronic structure and the magnetic properties of SrRuO_3 and CaRuO_3 . *J Phys Condens Matter* 9:9563-9584.
10. Mazin II & Singh DJ (1997) Electronic structure and magnetism in Ru-based perovskites. *Phys Rev B* 56(5):2556-2571.
11. Middey S, Mahadevan P, & Sarma DD (2011) Dependence of magnetism on GdFeO_3 distortion in the t_{2g} system ARuO_3 (A = Sr, Ca). *Phys Rev B* 83(1):014416.
12. Jin CQ, *et al.* (2008) High-pressure synthesis of the cubic perovskite BaRuO_3 and evolution of ferromagnetism in ARuO_3 (A = Ca, Sr, Ba) ruthenates. *Proc Natl Acad Sci USA* 105(20):7115-7119.
13. Shannon RD (1976) Revised effective ionic radii and systematic studies of interatomic distances in halides and chalcogenides. *Acta Cryst.* A32:751-767.

14. Ranjan R, *et al.* (2007) Structural stability of conducting oxide CaRuO₃ at high temperatures. *Appl Phys Lett* 90(25):251913-251913.
15. Kolesnik S, Dabrowski B, & Chmaissem O (2008) Structural and physical properties of SrMn_{1-x}Ru_xO₃ perovskites. *Phys Rev B* 78(21):214425.
16. Kiyama T, Yoshimura K, Kosuge K, Mitamura H, & Goto T (1999) High-field magnetization of Sr_{1-x}Ca_xRuO₃. *J Phys Soc Jpn* 68(10):3372-3376.
17. Zhou JS & Goodenough JB (2005) Universal octahedral-site distortion in orthorhombic perovskite oxides. *Phys Rev Lett* 94(6):065501.
18. Mountstevens EH, Attfield JP, & Redfern SAT (2003) Cation-size control of structural phase transitions in tin perovskites. *J Phys Condens Matter* 15(49):8315.
19. Howard CJ, Knight KS, Kennedy BJ, & Kisi EH (2000) The structural phase transitions in strontium zirconate revisited. *J Phys Condens Matter* 12(45):L677.
20. Griffiths RB (1969) Nonanalytic behavior above the critical point in a random Ising ferromagnet. *Phys Rev Lett* 23(1):17-19.
21. Salamon MB, Lin P, & Chun SH (2002) Colossal magnetoresistance is a griffiths singularity. *Phys Rev Lett* 88(19):197203.
22. Zhou JS, *et al.* (2008) Critical behavior of the ferromagnetic perovskite BaRuO₃. *Phys Rev Lett* 101(7):077206.
23. Gao L, *et al.* (1994) Superconductivity up to 164 K in HgBa₂Ca_{m-1}Cu_mO_{2m+2+δ} (m=1, 2, and 3) under quasihydrostatic pressures. *Phys Rev B* 50(6):4260-4263.